RSC Advances

ROYAL SOCIETY OF CHEMISTRY

www.rsc.org/advances

Cite this: DOI: 10.1039/c0xx00000x

www.rsc.org/xxxxxx

ARTICLE TYPE

A new application of oily cold rolling mill sludge for preparing Fe_2O_3/graphene as anodes for lithium-ion batteries

Cheng Liu[a,‡], Xinjing Wang[b,‡], Peng Ma[b], Jilu Chen[b], Jianzhong Jiang[b], Yani Ai[b], Erqin Wang[a], Sheng Han[b,*], Shaofeng Rong[a,*]

Received (in XXX, XXX) Xth XXXXXXXXX 20XX, Accepted Xth XXXXXXXXX 20XX
DOI: 10.1039/b000000x

Oily cold rolling mill sludge, which consists of iron and oil and hard to degrade, may cause problems in air or soil pollution. Therefore, the effective use of oily cold rolling mill sludge can not only reduce pollution but also produce environmental and economic benefits. In this research, the sludge was first used as the precursor to prepare LIB materials. As anode materials for lithium ion batteries, it showed a large reversible capacity of 560 mA h/g after 100 cycles at a small charge−discharge rate current of 100 mA/g as well as good rate capability of 508 and 380 mA h/g at ultrahigh current densities of 2000 and 5000 mA/g.

1. Introduction

The increasing demand for eco-environmental friendly industry has attracted great attention from both academic and industrial organizations to develop new processes and novel materials. Oily cold rolling mill (CRM) sludge, a by-product of steel making in the process of cold rolled strip production, is basically composed of metallic iron andiron oxides (70 wt%–90 wt%) with variable oil and grease (7 wt%–20 wt%)[1]. In the past, landfill and incineration were generally regarded as the simplest measure for the treatment of oil sludge, which may cause problems in air or soil pollution. Now, more and more pollution-free method was adopted to deal with oil sludge. It has also become an attractive alternative material for sustainable production given the depletion of iron ores and the rapid increase in the price of metal [2–6].

To avoid the environment pollution, oil-solid separation is the most commonly used method, such as pyrolysis[7–9], electro-demulsification[10], aqueous surfactant washing[11, 12], biological treatment[13], and distillation technology[14–16]. Regardless of the technologies adopted for oil sludge treatment, only a few studies[17] have maximized the use of iron resources in sludge.

Fe_2O_3/graphene composite is widely utilized in many fields, such as environmental protection [18, 19], sensor applications[20–22], and catalysis[23, 24]. It also widely used in lithium ion batteries (LIBs) and supercapacitors because of its high theoretical specific capacity, good cycling stability, and excellent rate capability. Yu et al. employed a facile one-step hydrothermal method to synthesize Fe_2O_3/graphene nanocomposites; after cycling at 200 mA/g for 450 cycles, a capacity of 1049 mA h/g can still be maintained[25]. Ning synthesized ~3 nm of Fe_2O_3 nanoparticles uniformly distributed in the nanopores of NMG as anodes for LIBs through an adsorption−precipitation process[26]. Hao et al. prepared Fe_2O_3/graphene nanocomposite through a one-step hydrothermal method and obtained high specific capacitance for supercapacitors[27]. Nevertheless, fewer people ever synthesized Fe_2O_3/graphene with the iron resources in sludge. Therefore, developing an efficient and viable method for the synthesis of Fe_2O_3/graphene using waste is not only a major challenge but also can produce environmental and economic benefits.

In this paper, we present a novel method called alkali liquor–ultrasound to deal with oily CRM sludge. The percentage of oil in the sludge was significantly reduced through this method. Then, by using the metal powder from the oily CRM sludge as a raw material, Fe_2O_3/graphene was fabricated through a hydrothermal process in a DMF-water co-solvent system. When Fe_2O_3/graphene was applied as LIB anodes, it allowed for high capacity, good cycling stability, and excellent rate capability because of the combined advantage of metal oxides and graphene.

2. Experimental

2.1. Chemical Materials

Oily CRM sludge was obtained from Shanghai Baosteel Group Corporation and graphite flakes were purchased from Sigma Aldrich (USA). $NaNO_3$, $KMnO_4$, 98% H_2SO_4, 30% H_2O_2, and N, N-dimethylformamide (DMF) were purchased from Sinopharm Chemical Reagent Co. Ltd. (Shanghai, China). All chemicals were of analytical grade and were used as received

without further purification.

2.2. Pretreatment of oily CRM sludge

A mixture with 20 g of oily CRM sludge and sodium hydroxide solution (5%) at a mass ratio of 1 to 6 was ultrasonicated and agitated for 20 min. The mixture was then poured into centrifuge tubes. After centrifugation at 8000 rpm for 20 min, the solid phase was segregated from the mixture. The solid phase was dried in an oven at 60 ℃ overnight, heated, and then kept at this temperature for 12 h.

2.3. Synthesis of Fe_2O_3/graphene nanocomposites

A total of 1.5 g of the solid phase and 8 mL H_2SO_4 (98%) were mixed and heated at 120 ℃ for 10 h. Then, 200 mL of distilled water was added for dilution. The iron source solution was segregated from the mixture after centrifugation at 8000 rpm for 30 min, followed by gradually adding a 10% aqueous solution of sodium hydroxide solution to adjust the pH to 3-4. Graphene oxide (GO) was synthesized from natural graphite flakes through a modified Hummers method[28, 29]. 30 mL of graphene oxide (GO, 450 mg/L) aqueous dispersion and 50mL DMF were ultrasonicated with 20 mL of the iron source solution for 30 min to form a homogeneous suspension. At this time, 3 mL of H_2O_2 was added to accelerate oxidation. The stable suspension was then sealed in a teflon-lined autoclave and hydrothermally treated at 180 ℃ for 12 h. After cooling to room temperature, the as-prepared sample was centrifuged, washed with distilled water three times, and then freeze dried for 24 h. For comparison, pure Fe_2O_3 samples was also prepared by the same procedure without graphene.

2.4. Material characterizations

The morphology and structure of the samples was characterize with a field-emission scanning electron microscope (FESEM, Hitachi, S-4800N), a transmission electron microscope (TEM, JEOL, JEM−2010) and powder X-ray diffraction(XRD, PANalytical B.V, PW3040/60) with Cu−Kα irradiation (λ = 0.15406 nm) at 40 kV (20 mA) at 2θ range from 10° to 80°. The elemental analysis of the samples was investigated by X-ray fluorescence spectrometer (XRF, ARL, 9800XP). Roman spectra were obtained with a Senterra R200-L multichannel confocal micro spectrometer with 532 nm laser excitation. Thermogravimetric analysis (TGA) was conducted with TA Q5000IR at a heating rate of 10 ℃ min^{-1} under flowing air. Nitrogen adsorption/desorption isotherms at 77 K were determined by Micrometrics SAP 2010.

2.5. Electrochemical measurements

The electrochemical properties of the samples were evaluated with CR 2016 coin cells at room temperature. The test electrodes consisted of active materials (80%), conductive carbon black (super P) as the conductive agent (10%), and polyvinylidene fluoride (PVDF) dissolved in N-methyl-2-pyrrolidone (NMP) as the binder (10%) to form a slurry. The slurry was then coated onto copper foil with a thickness of 100 mm, and then punched into disks with a diameter of 13 mm as the test electrode. The total material loading was 0.8 mg cm^{-2}. Celgard 2400 microporous polypropylene membrane and pure lithium foil were used as separator and counter electrode, respectively. The electrolyte consisted of a solution of 1 M LiPF6 in ethylene carbonate-dimethyl carbonate−diethyl carbonate (1:1:1, in wt %). The CR 2016 coin cells were assembled in an argon-filled glove box with water and oxygen contents less than 1 ppm. The discharge and charge measurements were evaluated with LAND 2001A system, with the cut off potentials being 0.01 V for discharge and 3.0 V for charge. All the specific capacities reported and current densities used were based on the total electrode weight. Electrochemical impedance spectroscopy (EIS) was performed on a CHI760D electrochemical workstation by applying a sine wave with an amplitude of 5 mV in the frequency range 100 kHz to 0.01 Hz.

3. Results and discussion

3.1. Solid phase

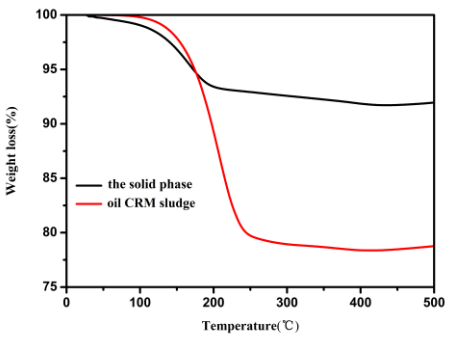

Figure 1. TGA curves for solid phase and oily CRM sludge in the air

TGA measurement conducted in the air was utilized to determine the percentage of oil in the solid phase. As shown in Figure 1 and Table S1, the TGA curve were divided into four stages and the mainly weight loss is in second stage. First stage, the miniscule weight loss of the solid phase (<1%) and oily CRM sludge (2%) appeared at approximately 25-120 ℃, indicating the combustion of water. The next stage at 120-200 ℃ and 120-250 ℃ was the significant weight loss of the solid phase and oily CRM sludge which was approximately 6% and 20%, respectively, indicating the combustion of the oil. The third stage was a stationary phase. In the fourth stage, there was a slight weight increase (<1%) that appeared at approximately 400-500 ℃ was attributed to the oxide of iron. Therefore, we concluded that the content of oil in sludge decreased from 20% to 6% through the proposed alkaline liquor–ultrasound method. The content of metals in the solid phase was estimated through XRF. Figure 1 and Table 1 showed that the sample predominantly contains Fe (74.6 wt%) and small amounts of Cr, Mn, Ni, and Cu.

Table 1 Composition Analysis of the solid phase, % by Mass

P	Ca	Mn	Fe	Cr	Ni	Cu	Zn
<0.1	<0.1	2.0	74.6	4.6	1.0	0.5	<0.05

3.2. Fe_2O_3/graphene nanocomposites

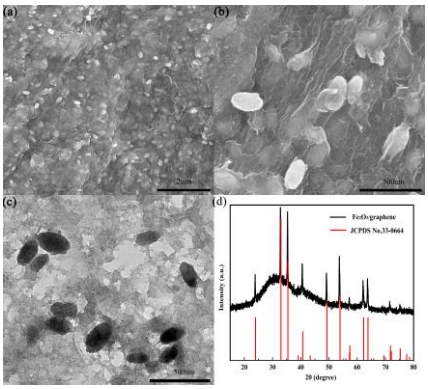

Figure 2. (a, b) FESEM images, (c) TEM images, (d) XRD spectrum of Fe_2O_3/graphene.

The morphology and microstructure of the as-prepared Fe_2O_3/graphene were elucidated by means of FESEM and TEM. The low-magnification image in Figure 2a showed a complete picture, which consists of a thin, wrinkled, "paper-like" structure. The high-magnification SEM image in Figure 2b showed that the Fe_2O_3 nanoparticles were uniformly distributed on the surface of graphene. Most Fe_2O_3 particles were encapsulated within the graphene sheets, which can efficiently prevent the aggregation of particles and avoid direct contact between Fe_2O_3 particles and electrolytes.

The typical Fe_2O_3 particle size was 200–400 nm in diameter, which can be further confirmed by the TEM image in Figure 2c. The crystal structure of the iron oxide nanoparticles in the nanocomposite was characterized by powder X-ray diffraction (Figure 2d). Apparently, all the intense peaks can be well indexed to hematite Fe_2O_3 (JCPDS No. 33-0664), indicating that the crystallization of Fe_2O_3 during the hydrothermal treatment was not affected by the addition of GO sheets. No apparent diffraction peaks from graphene or graphene oxide were detected because of the ultrathin characteristic of the graphene sheets in the products[30].

In order to explore specific surface area and the porous structure of Fe_2O_3/graphene, N_2 adsorption–desorption analysis have been carried out(Figure S1(a, b)). The surface area of Fe_2O_3/graphene reached up to 175m^2/g, which contrasted markedly to that of pure Fe_2O_3, and the pore volume was 0.1cm^3/g for Fe_2O_3/graphene. This result revealed that graphene coated was an effective way to achieve a high surface area. Moreover, based on the Barret Joyner Halenda (BJH) calculation, the average pore size was 2.5nm. The high porosity can provide not only more surface reaction sites but also enough space to slow down the volume expansion of Fe_2O_3 during lithiation and delithiation, and was therefore favorable for the electrochemical properties[31].

The synthesis of the Fe_2O_3 /graphene can be described as follows: First, $Fe(OH)_3$ colloid was generated after NaOH and H_2O_2 was added into the iron source solution. As was well known from colloidal science[32], hydroxide colloid are typically positively charged due to the adsorption of cations, while GO was negatively charged due to the presence of oxygen-containing groups. In this case, the combination of $Fe(OH)_3$ and GO afforded a tight and uniform $Fe(OH)_3$ deposition on the surface of GO. Then, when the mixture was hydrothermally treated at 180 ℃, GO was reduced to graphene sheets[33] accompanying with in situ transformation of $Fe(OH)_3$ to Fe_2O_3 in DMF. And the chemical reaction equations can be represented as follows:

$Fe^{2+}+OH^-=Fe(OH)_2$

$Fe(OH)_2+H_2O_2= Fe(OH)_3+H_2O$

$Fe(OH)_3=Fe_2O_3+H_2O$

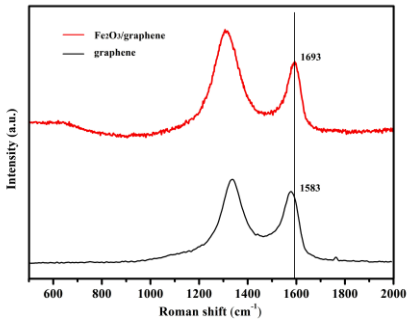

Figure 3. Raman spectrum of Fe_2O_3/graphene

The Raman spectra of GO and Fe_2O_3/graphene are shown in Figure 3. The peak at about 1590 cm^{-1} (G band) corresponding to an E_{2g} mode of graphite is related to the vibration of sp^2 hexagonal lattice, whereas the peak at about 1340 cm^{-1} of bonded carbon atoms in a 2D (D band) is related to the defects and disorders in the hexagonal graphitic layers[34, 36]. In this study, the intensity ratio of D/G bands for GO was 1.17; it increased to 1.47 for Fe_2O_3/graphene. The enhancement in the D/G ratio suggests an increase in the number of sp2 domains in Fe_2O_3/graphene and confirms the reduction in GO[36, 37] and the presence of Fe_2O_3 nanoparticles[38]. The G peak of α-Fe_2O_3/graphene shifted to 1693 cm^{-1} compared with GO (1583cm^{-1}), which exhibited a 10 cm^{-1} blue shift. This phenomenon can be explained by the charge transfer between carbon materials and nanomaterials[39–42].

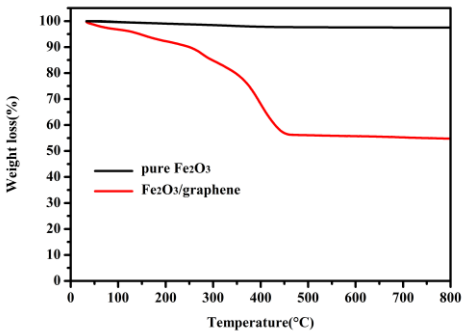

Figure 4. TGA curves of pure Fe_2O_3 and Fe_2O_3/graphene

Fe_2O_3/graphene was characterized through TGA measurement carried out in air to determine its chemical composition. As shown in Figure 4, the TGA curve of Fe_2O_3 displayed a significant weight loss of about 300 ℃ and a constant weight of above 450 ℃. The major weight loss at 300 ℃ to 450 ℃ was approximately 35%, indicating the oxidation of graphene[38]. The weight loss below 300 ℃ was attributed to the

evaporation of unstable organic species as well as adsorbed water molecules[43, 44]. In a typical process, the weight loss below 300 ℃ is miniscule(<1%), but in this experiment, the proportion of this part is relatively large(10%), which may be resulting from the impurity in raw material. Therefore, the mass percentage of Fe_2O_3 in Fe_2O_3/graphene was calculated to be 55%.

3.3 Electrochemical properties

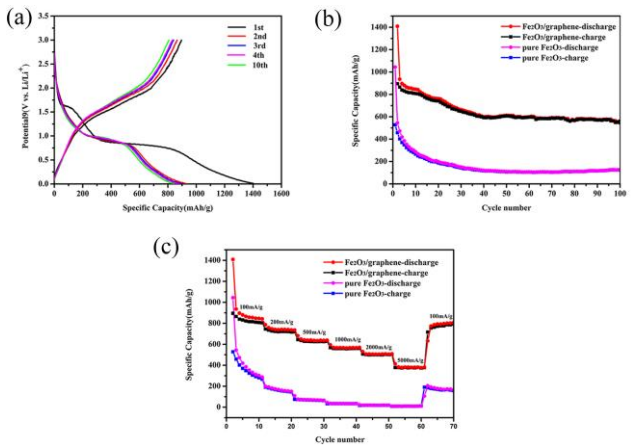

Figure 5. (a) Discharge/charge profiles of Fe_2O_3/graphene at the current density of 100 mA/g between 0.01 and 3.0 V: the discharge curves in the first, second, third, fourth and tenth cycles, (b) Cycling performance of Fe_2O_3/graphene and pure Fe_2O_3 at the current density of 100 mAg/g, (c) Rate capacity of Fe_2O_3/graphene and pure Fe_2O_3 between 0.01 and 3.0 V with increasing current density.

The electrochemical performance of the as-prepared Fe_2O_3/graphene was evaluated through galvanostatic discharge−charge (Li insertion–Li extraction) cycling in a cell by using lithium metal as the counter electrode at a current density of 100 mA/g between 0.01 and 3 V (Figure 5a). The first discharge profile was divided into three: $Fe_2O_3 \rightarrow Li_xFe_2O_3 \rightarrow$ cubic $Li_2Fe_2O_3 \leftrightarrow Fe + Li_2O$. The first stage at 1.6 V was caused by the phenomenon that a small amount of lithium ions was inserted into the Fe_2O_3 crystal structure[45, 46]. The next stage at 1.0 V was clearly observed and was found to be related to the decomposition of the electrolyte and the formation of a solid-electrolyte interface (SEI) layer[47]. The last stage corresponded to the transformation of Fe^{2+} to Fe^0 [45, 46].

The initial discharge capacity of Fe_2O_3/graphene was 1400 mA h/g, and the charging capacity was 895 mA h/g with an initial Coulombic efficiency of 64% (Figure 5a). The irreversible capacity loss (36%) can be ascribed to the formation of solid electrolyte interface (SEI) layer on the surface of the electrode during initial discharge[48]. The coulombic efficiency remained near 99% after 10 cycles, indicating the stability of the SEI film and the good reversibility of the electrochemical reactions[49, 50].

Figure 5b shows the cycling performance of Fe_2O_3/graphene and pure Fe_2O_3 at a small, constant current rate of 100 mAh/g. After 100 cycles, the discharge capacity of the Fe_2O_3/graphene was still close to 560 mAh/g, which was much higher than the theoretical specific capacity of graphene (372 mAh/g). Compared with pure Fe_2O_3, which only delivered a reversible capacity of 100 mA h/g after 100 cycles, it displayed good charge and discharge cycles. It could be ascribed to two reasons. First, the volume of the pure Fe_2O_3 increased sharply during lithiation and led to a reduction in capacity[51]. The second reason was the positive contribution of the graphene nanosheet support. Using graphene as anodes for Li ion batteries has a positive influence on the performance of Fe_2O_3. Graphene provided not only a large specific surface area for the insertion and extraction of lithium ions but also mechanical flexibility to cushion the volume change of Fe_2O_3 anodes during cycling [52–54].

In addition to its good performance rate, Fe_2O_3/graphene also exhibited excellent rate capability. The rate performance was evaluated by cycling the electrode 10 times at each of the six different current densities (from 0.1 A to 5 A). The representative cycling data were shown in Figure 5c. It was clearly seen that the Fe_2O_3/graphene illustrate much better rate performances comparing to the reference pure Fe_2O_3. The discharge capacities of the Fe_2O_3/graphene were maintained at 842, 736, 639, and 570 mAh/g at current densities of 100, 200, 500, and 1000 mA/g, respectively. Even at ultrahigh current densities of 2000 and 5000 mA/g, the discharge capacities remained at 508 and 380 mAh/g, corresponding to 60% and 46% retention, compared with 100 mA/g. In addition, when the current density was reduced back to the initial 100 mA/g after the high rate test, the discharge capacities recovered to 790 mAh/g, which indicated excellent rate performance. However, the pure Fe_2O_3 electrode displayed a noticeably poor rate capability with the increased current densities and the capacity retention is only about 20% after 70 cycles. EIS measurements were carried out, which can make us to gain insight into the electrochemical performances of Fe_2O_3/grapheme. Figure S2 showed the Nyquist plots of Fe_2O_3/graphene and pure Fe_2O_3. As can be seen from the figure, the diameter of the semicircle for the Fe_2O_3/grapheme electrode in the high-to-medium-frequency region was much smaller than the pure Fe_2O_3, suggesting that the existence of graphene improves the conductivity of pure Fe_2O_3 a lot[55]. As a result, the Fe_2O_3/grapheme performed a better electrochemical properties than the pure Fe_2O_3.

The high capacity, good cycling stability, and excellent rate capability of Fe_2O_3/graphene can be attributed to the following factors. First, the small size of the iron oxide nanoparticles accelerated the exchange speed of electrons and lithium irons. Second, the embedded structure between Fe_2O_3 particles and graphene prevented the aggregation of iron oxide and accommodated its volume expansion during cycling. Third, the high dispersion of Fe_2O_3 on graphene efficiently reduced the diffusion length for both electrons and lithium ions.

4. Conclusions

In summary, a novel method called alkali liquor–ultrasound was developed to deal with oily CRM sludge. The oil content of the sludge was reduced from 20% to 7%, and the state of the sludge changed from black viscous liquid to solid powder. Fe_2O_3/graphene was fabricated using the solid powder and graphene via a hydrothermal process in a DMF-water co-solvent system. When the Fe_2O_3/graphene was applied as LIB anodes, they provided an outstanding enhancement of capacity and rate performance, with a very high capacity of 1400 and 380 mA h/g

at a high rate of 5000 mA/g. The proposed synthetic strategy can be further extended to develop other waste metal materials used as lithium battery.

Acknowledgements

This project was supported by the Shanghai Leading Academic Discipline Project (Project Number J51503), National Natural Science Foundation of China (Project Number 20976105), Science and Technology Commission of Shanghai Municipality (Project Number 09QT1400600), Innovation Program of Shanghai Municipal Education Commission (Project Number 11ZZ179) and Innovation Program of Shanghai Municipal Education Commission (Project Number 09YZ387), Shanghai Talent Development Funding (Project Number 201335).

Notes and references

[a] *School of Perfume and Aroma Technology, Shanghai Institute of Technology, Shanghai 201418, China. *Co-corresponding author E-mail: rongshaofeng@163.com; Tel: +86 13818786015;*
[b] *School of Chemical and Environmental Engineering, Shanghai Institute of Technology, Shanghai 201418, China. *Corresponding author Email: hansheng654321@sina.com; Tel: +86 13524694909;*
‡ *These two authors contributed equally to this work.*

1 B. Liu, S. G. Zhang, J. J. Tian, D. A. Pan, Y. Liu, A. A. Volinsky, *Int. J. Miner. Metall. Mater*, 2013, **20**, 941.

2 C. Li, H. H. Sun, J. Bai, L.T. Li, *J. Hazard. Mater*, 2010, **174**, 71

3 Y. S. Sun, Y. X. Han, P. Gao, Z. H. Wang, D. Z. Ren, *Int. J. Miner. Metall. Mater*, 2013, **20**, 411.

4 Y. L. Zhang, H. M. Li, X. J. Yu, *J. Hazard. Mater*, 2012, **213**, 167

5 K. Jayasankar, P. K. Ray, A. K. Chaubey, A. Padhi, B. K. Satapathy, P. S. Mukherjee, *Int. J. Miner. Metall. Mater*, 2012, **19**, 679.

6 Z. L. Yi, H. H. Sun, X. Q. Wei, C. Li, *Int. J. Miner. Metall. Mater*, 2009, **16**, 355.

7 H. Schmidt, W. Kaminsky, *Chemosphere*, 2001, **45**, 285.

8 J. L. Shie, C. Y. Chang, J. P. Lin, D. J. Lee, C. H. Wu, *Energy. fuel*, 2002, **16**, 102.

9 J. L. Shie, J. P. Lin, C. Y. Chang, S. M. Shih, D. J. Lee, C. H. Wu, *J. Anal. Appl. Pyrolysis*, 2004, **71**, 695.

10 M. Elektorowicz, S. Habibi, R. E. J. Chifrina, *Colloid. Interface. Sci*, 2006, **295**, 535.

11 J. I. Chang, J. J. Lin, J. S. Huang, Y. M. Chang, *Resour. Conserv. Recycl*, 2006, **49**, 191.

12 B. Ruffino, M. C. Zanetti, *Resour. Conserv. Recycl*, 2008, **52**, 1315.

13 B. Mrayyan, M. N. Battikhi, *J. Hazard. Mater*, 2005, **120**, 127.

14 H. C. Eun, H. C. Yang, Y. Z. Cho, H. S. Lee, I. T. Kim, *J. Hazard. Mater*, 2008, **160**, 634.

15 Y. H. Zhou, W. B. Wu, K. Q. Qiu, *Waste. Manage*, 2010, **30**, 2299.

16 K. H. Lin, H. T. Hsu, Y. W. Ko, Z. X. Shieh, H. L. Chiang, *J. Hazard. Mater*, 2009, **171**, 208.

17 Bo. Liu, S. G. Zang, J. J. Tian, D. A. Pan, H. X. Zhu. *Rare. metals*, 2013, **32**, 518.

18 S. Vadahanambi, S. H. Lee, W. J. Kim, I. K. Oh, *Environ. Sci. Technol*, 2013, **47**, 10510.

19 A. P. Singh, M. Mishra, P. Sambyal, B. K. Gupta, B. P. Singh, A. Chandra, S. K. Dhawan, *J. Mater. Chem. A*, 2014, **2**, 3581.

20 S. Radhakrishnan, K. Krishnamoorthy, C. Sekar, J. Wilson, S. J. Kim, *Appl. Catal. B-Environ*, 2014, **148**, **22**.

21 S. Liang, J. Zhu, C. Wang, S. Yu, H. Bi, X. Liu, X. Wang, *Appl. Surf. Sci*, 2014, **292**, 278.

22 Z. Jiang, J. Li, H. Aslan, Q. Li, Y. Li, M. Chen, Y. Huang, J. P. Froning, M. Otyepka, R. Zbořil, F. Besenbacher, M. Dong, *J. Mater. Chem. A*, 2014, **2**, 6714.

23 Y. Yuan, W. Jiang, Y. Wang, P. Shen, F. Li, P. Li, F. Zhao, H. Gao, *Appl. Surf. Sci*, 2014, **303**, 354.

24 G. K. Pradhan, D. K. Padhi, K. M. Parida, *ACS. Appl. mater. inter*, 2013, **5**, 9101.

25 H. Zhang, L. Zhou, C. Yu, *RSC. Adv*, 2014, **4**, 495.

26 X. Zhu, X. Song, X. Ma, G. Ning, *ACS. Appl. mater. inter*, 2014, **6**, 7189.

27 Z. Wang, C. Ma, H. Wang, Z. Liu, Z. Hao, *J. Alloy. Compd*, 2013, **552**, 486.

28 W. S. Hummers, R. E. Offeman, *J. Am. Chem. Soc*, 1958, **80**, 1339.

29 Y. Y. Liang, D. Q. Wu, X. L. Feng, K. Müllen, *Adv. Mater*, 2009, **21**, 1679.

30 L. Xiao, D. Q. Wu, S. Han, Y. Huang, S. Li, M. He, F. Zhang, X. L. Feng, *ACS. appl. mater. inter*, 2013, **5**, 3764.

31 C. F. Zhang, Z. X. Chen, Z. P. Guo, X. W. Lou, *Energy. Environ. Sci*, 2013, **6**, 974.

32 R. Wang, C. Xu, M. Du, J. Sun, L. Gao, P. Zhang, H. Yao, C, Lin, Small, 2014, 10, 2260.

33 R. H. Wang, Y. Wang, C. H. Xu, J. Sun, L. Gao, Rsc Adv. 2013, 3, 1194.

34 M. X. Chen, C. C. Zhang, X. C. Li, L. Zhang, Y. L. Ma, L. Zhang, X. Y. Xu, F. L. Xia, W. Wang, J. P. Gao, *J. Mater. Chem. A*, 2013, **1**, 2869.

35 F. Tuinstra, J. L. Koenig, *J. Chem. Phys*, 1970, **53**, 1126.

36 Y. Gu, Y. Xu, Y. Wang, *ACS Appl. Mater. Interfaces*, 2013, **5**, 801−806.

37 Z. Y. Sui, X. T. Zhang, Y. Lei, Y. J. Luo, *Carbon*, 2011, **49**, 4314.

38 M. Zhang, B. Qu, D. Lei, Y. Chen, X. Yu, L. Chen, Q. Li, Y. Wang, T. Wang, *J. Mater. Chem*, 2012, **22**, 3868.

39 G. Zhou, D. W. Wang, L. C. Yin, N. Li, F. Li, H. M. Cheng, *ACS Nano*,2012, **6**, 3214.

40 J. Zhou, H. Song, L. Ma, X. Chen, *RSC Adv*, 2011, **1**, 782.

41 S. Niyogi, E. Bekyarova, M. E. Itkis, H. Zhang, K. Shepperd, J. Hicks, M. Sprinkle, C. Berger, C. N. Lau, W. A. deHeer, E. H. Conrad, R. C. Haddon, *Nano. Lett*, 2010, **10**, 4061.

42 M. S. Dresselhaus, A. Jorio, M. Hofmann, G. Dresselhaus, R. Saito, *Nano. Lett*, 2010, **10**, 751.

43 W. F. Chen, S. R. Li, C. H. Chen, L. F. Yan, *Adv Mater*, 2011, **23**, 5679.

44 C. Z. Zhu, S. J. Guo, Y. X. Fang, S. J. Dong, *ACS Nano*, 2010, **4**, 2429.

45 L. Zhou, H. Y. Xu, H. W. Zhang, J. Yang, S. B. Hartono, J. Zou, C. Z. Yu, *Chem. Commun*, 2013, **49**, 8695.

46 W. J. Yu, P. X. Hou, F. Li, C. Liu, *J. Mater. Chem*, 2012, **22**, 13756.

47 Z. Wang, D. Luan, S. Madhavi, Y. Hu, X. W. D. Lou, *Energy Environ. Sci*, 2012, **5**, 5252.

48 J. J. Zhang, T. Huang, Z. L. Liu, A. S. Yu, *Electrochem. Commun*, 2013, **29**, 17.

49 F. Han, W. C. Li, M. R. Li, A. H. Lu, *J. Mater. Chem*, 2012, **22**, 9645.

50 F. Han, D. Li, W. Li, C. Lei, Q. Sun, A. Lu, *Adv. Funct. Mater*, 2012, **23**, 1692.

51 J. Lin, A. R. O. Raji, K. Nan, Z. Peng, Z. Yan, E. L. G. Samuel, D. Natelson, J. M. Tour, *Adv. Funct. Mater*, 2014, **24**, 2044.

52 D. Z. Chen, W. Wei, R. N. Wang, J. C. Zhu, L. Guo, *New J. Chem*, 2012, **36**, 1589.

53 D. Q. Wu,; F. Zhang,; H. W. Liang, X. L. Feng, *Chem. Soc. Rev*, 2012, **41**, 6160.

54 D. Q. Wu, F. Zhang, P. Liu, X. L. Feng, *Chem. Eur. J*, 2011, **17**, 10804.

55 H. Xiang, K. Zhang, G. Ji, J. Y. Lee, C. Zou, X. Chen, J. Wu, *Carbon*, 2011, **49**, 1787.

A new application of Oily cold rolling mill sludge for preparing Fe_2O_3/graphene as anodes for lithium-ion batteries

Cheng Liu[a,‡], Xinjing Wang[b,‡], Peng Ma[b], Jilu Chen[b], Jianzhong Jiang[b], Yani Ai[b], Erqin Wang[a], Sheng Han[b,*], Shaofeng Rong[a,*]

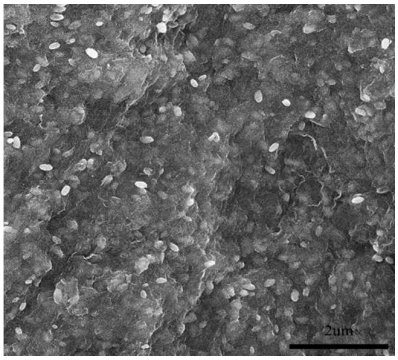

A new application of Oily cold rolling mill sludge in ithium-ion batteries